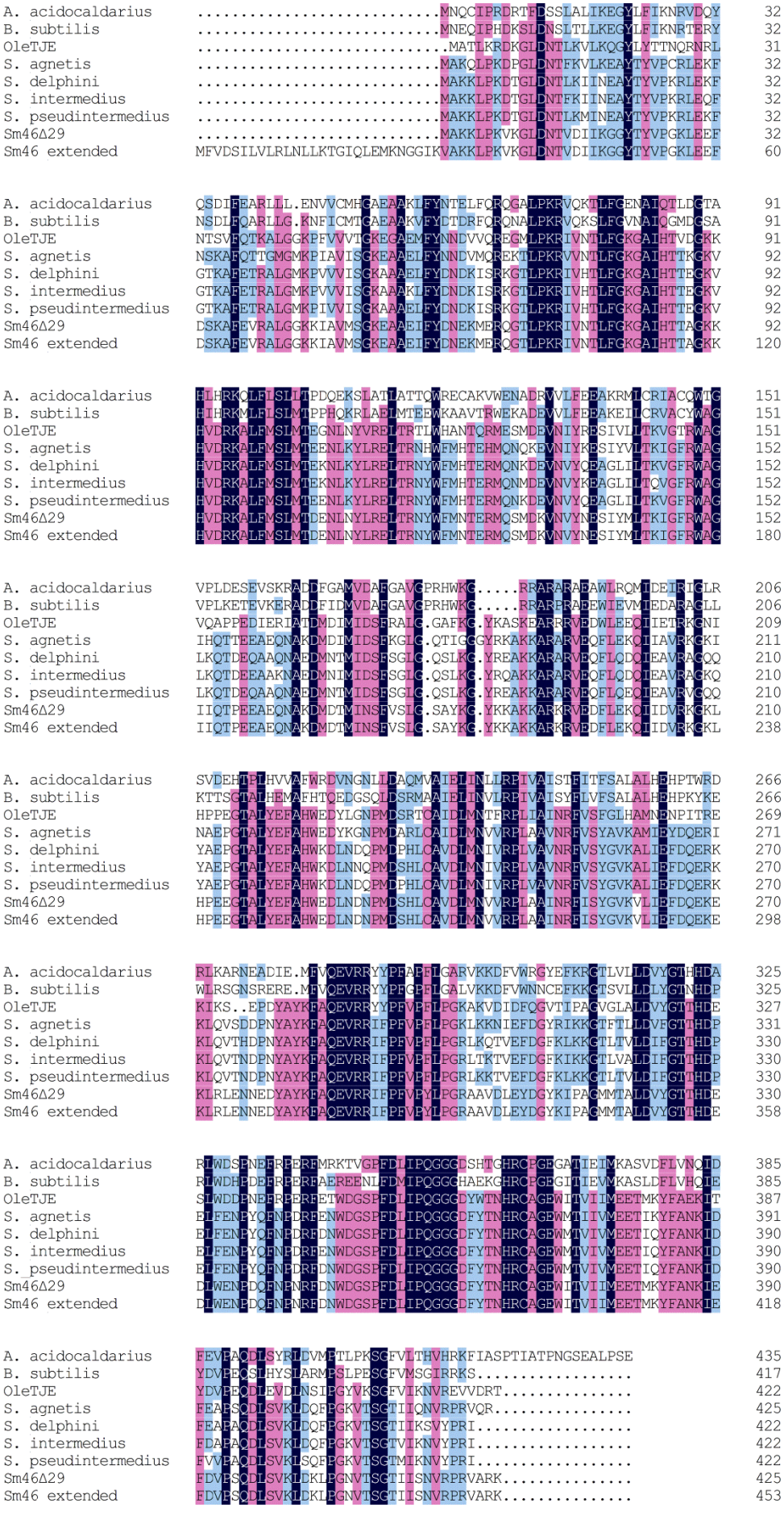
A. acidocaldarius
B. subtilis
OleTJE
S. agnetis
S. delphini
S. intermedius
S. pseudintermedius
Sm46Δ29
Sm46 extended

Figure S1. Protein sequence alignment of CYP-Aa162 from *A. acidocaldarius* (GenBank accession number: WP_008340313), $P450_{BS\beta}$ from *Bacillus subtilis str. 168* (GenBank accession number: NP_388092), $OleT_{JE}$ from *Jeotgalicoccus sp.* ATCC 8456 (GenBank accession number: ADW41779), CYP-Sm46 (labelled as Sm46 extended) from *Staphylococcus massiliensis* S46 (GenBank accession number: EKU50422), CYP-Sm46Δ29 (labelled as Sm46Δ29) from *S. massiliensis* (GenBank accession number: WP_039990689) and cytochrome P450 enzymes from other *Staphylococcus* species such as *S. agnetis* (GenBank accession number: KFE42911), *S. delphini* (GenBank accession number: WP_019165531), *S. intermedius* (GenBank accession number: WP_019167377) and *S. pseudintermedius* HKU10-03 (GenBank accession number: ADV05454).

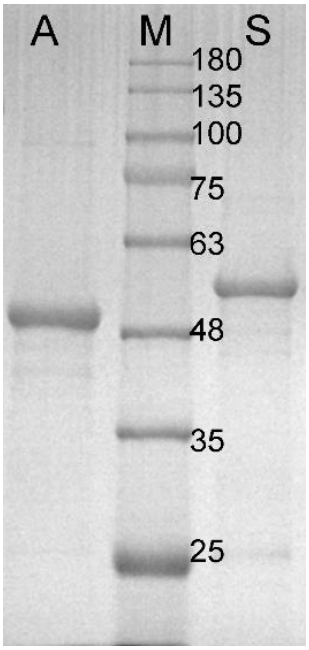

Figure S2. SDS-PAGE showing the purified His-tagged CYP-Aa162 (lane A) and CYP-Sm46Δ29 (lane S). Molecular sizes of the marker bands (lane M), from top to bottom, are 180, 135, 100, 75, 63, 48, 35 and 25 kDa respectively.

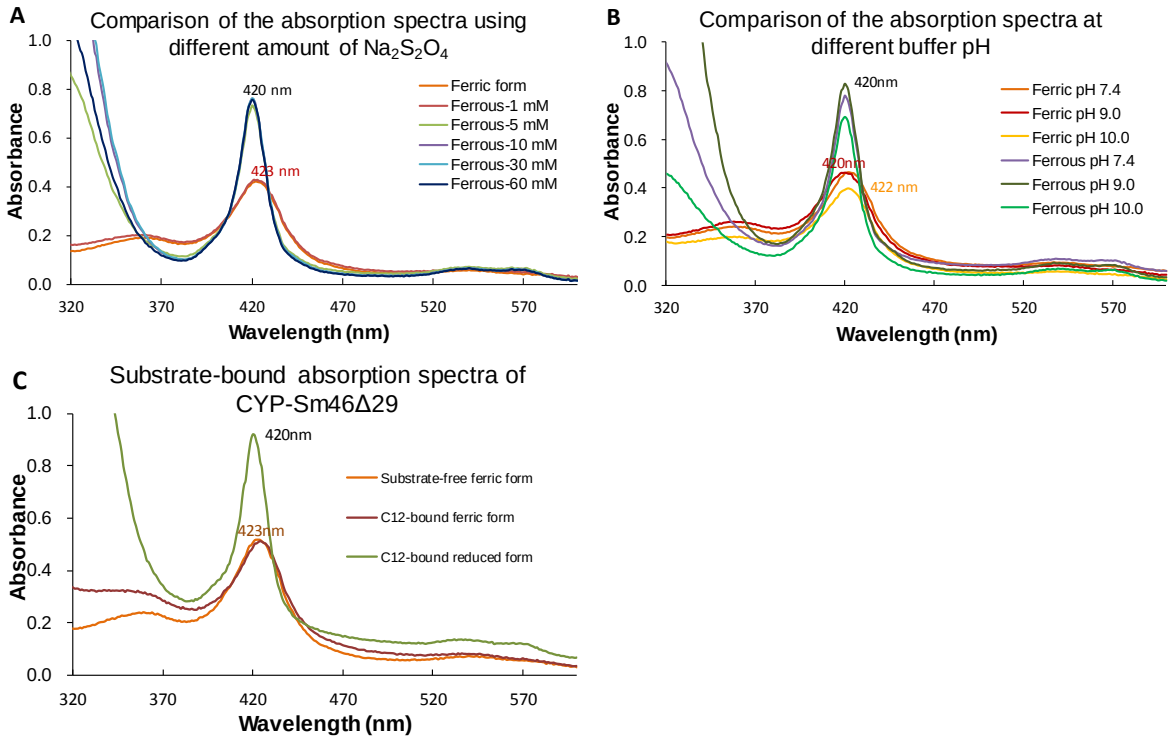

Figure S3. The UV-visible spectra of CYP-Sm46Δ29 (5 μM) under different conditions. (A) The purified CYP-Sm46Δ29 was diluted in 50 mM Na_3PO_4 (pH 7.4) buffer containing 300 mM NaCl and 10% glycerol. Spectra are shown for the oxidized ferric form of the enzyme (orange line) and the ferrous-CO complex reduced by the indicated amount of $Na_2S_2O_4$. (B) The purified CYP-Sm46Δ29 was diluted in 50 mM Na_3PO_4 buffer containing 300 mM NaCl and 10% glycerol with different buffer pH as indicated. Then the absorption spectra were recorded respectively for the oxidized ferric form and the ferrous-CO adduct reduced by 10 mM $Na_2S_2O_4$. The protein precipitates at buffer pH lower than 7.0. (C) A molar excess (600 μM) of C_{12} lauric acid was pre-incubated with the enzyme at room temperature for 5 min before the absorption spectra were recorded. Binding of C_{12} FA did not seem to induce an apparent spin-state transition of the ferric heme. The Soret peak of the C_{12}-bound ferrous-CO adduct of the enzyme was still detected at 420 nm.

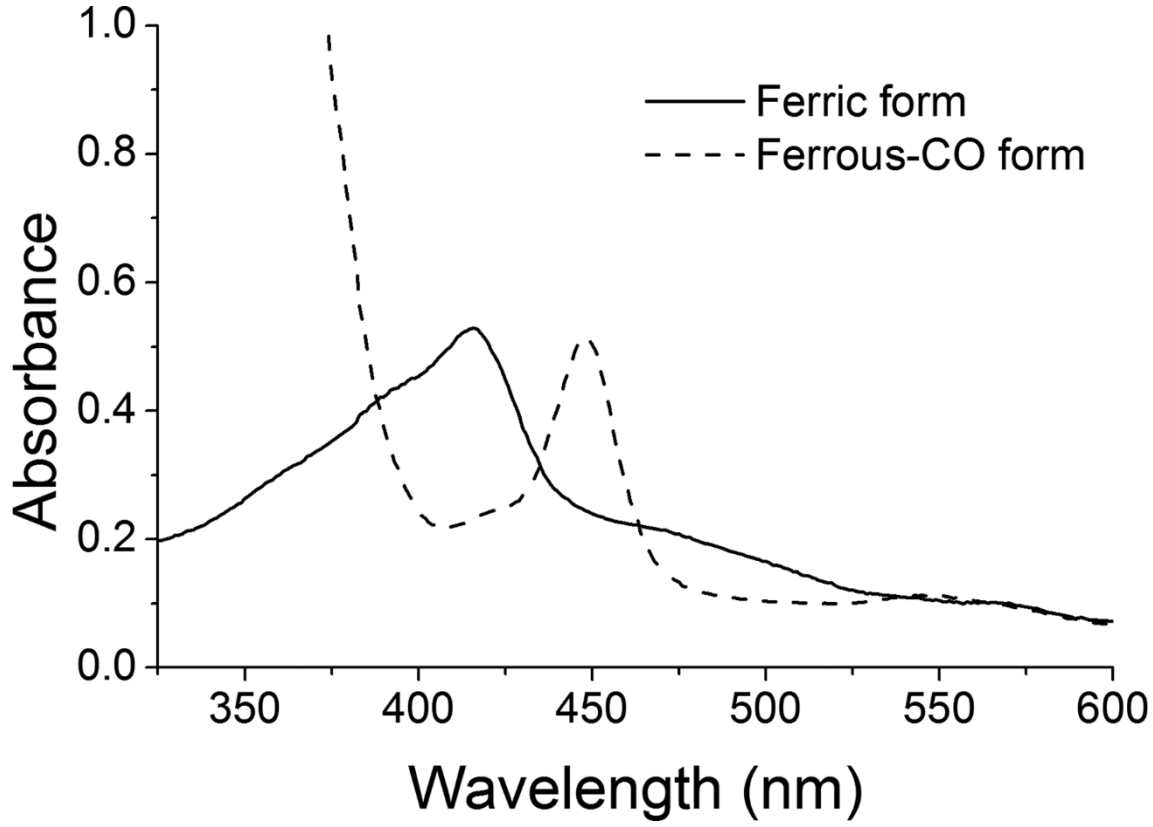

Figure S4. UV-visible spectra of the self-sufficient monooxygenase $P450_{BM3}$. The substrate-bound ferric form of $P450_{BM3}$ (solid line) shows a Soret maximum at ~ 416 nm with undistinguishable *β*-band and a weaker *α*-band at 570 nm. The reduced ferrous-CO form of $P450_{BM3}$ (dashed line) generated by the subsequent NADPH-initiated electron transfer features a shifted Soret peak to 448 nm.

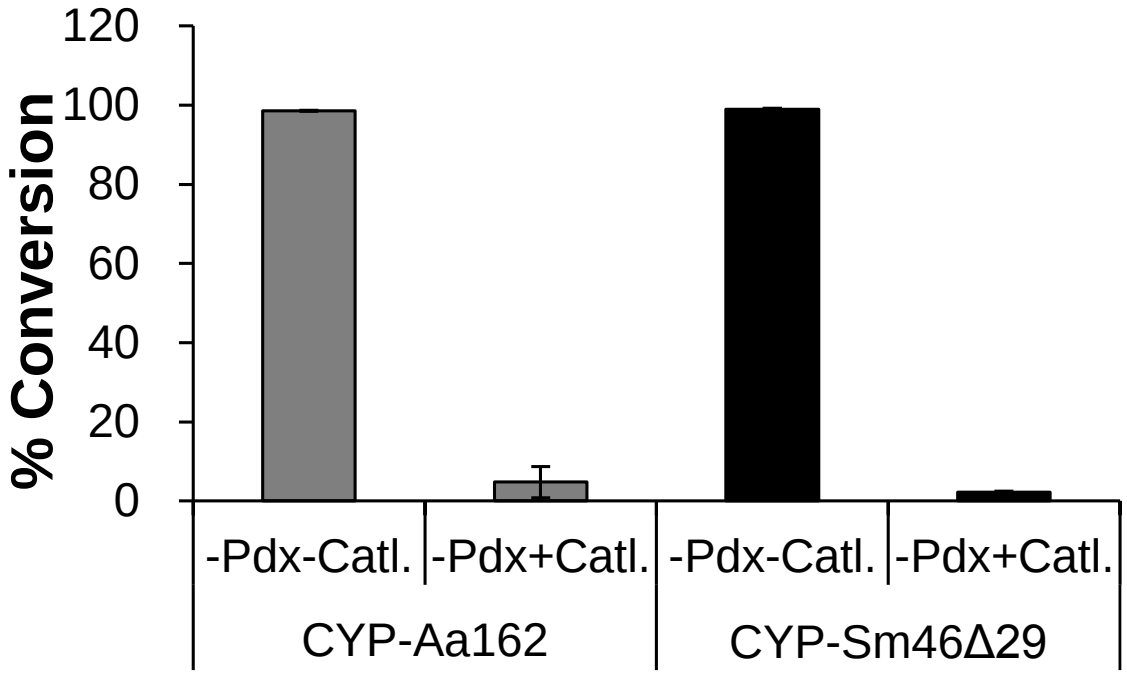

Figure S5. Effect of decoupling NADH oxidation and electron transfer on the catalytic conversion of lauric acid (LA) by CYP-Aa162 and CYP-Sm46Δ29. The reactions contained 0.2 mM LA, 2.0 μM CYP-Aa162 (or CYP-Sm46Δ29), 3.0 μM putidaredoxin reductase (PdR), 1 mM NADH in the absence and presence of 1200 U/ml catalase (Catl.). By subtracting putidaredoxin (Pdx) from the reaction system, the NADH oxidation was mandatorily decoupled from the Class I electron transfer chain to P450 enzymes. Any catalytic activity observed should be supported by the H_2O_2 generated from NADH oxidation and O_2 reduction. The percentage conversion of LA was determined by calculating the substrate consumption based on GC analysis. Results shown are mean ± SD of duplicated experiments.

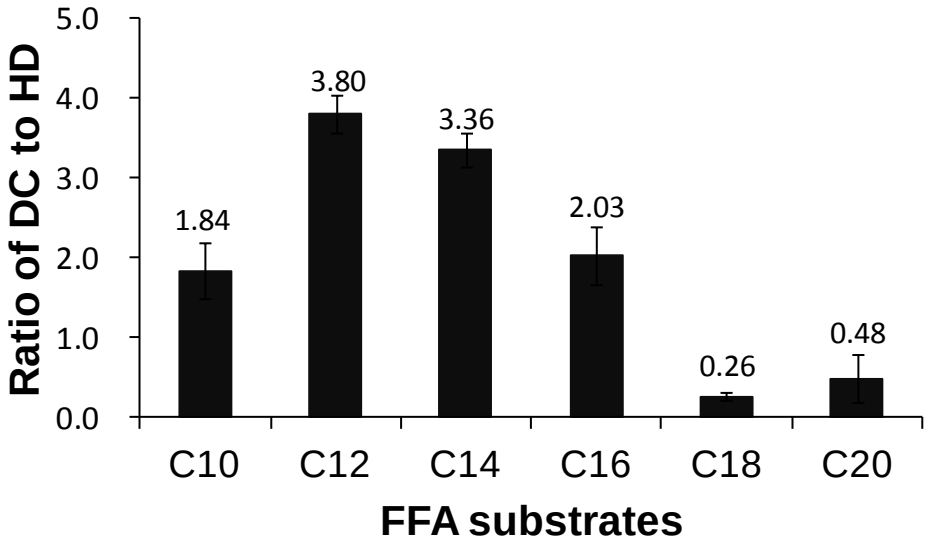

Figure S6. The ratios of free fatty acid (FFA) decarboxylation (DC) over hydroxylation (HD) by CYP-Sm46Δ29 against different FFA substrates. The decarboxylation activity was measured by detecting the 1-alkene yield using GC analytical method. The hydroxylation activity was estimated by subtracting the alkene production from the total substrate conversion. This indirect but more convenient method was validated with C_{14} myristic acid substrate by direct measurement of the BSTFA/TMCS derivatized hydroxylation products. Results are shown as mean ± SD of duplicated experiments.

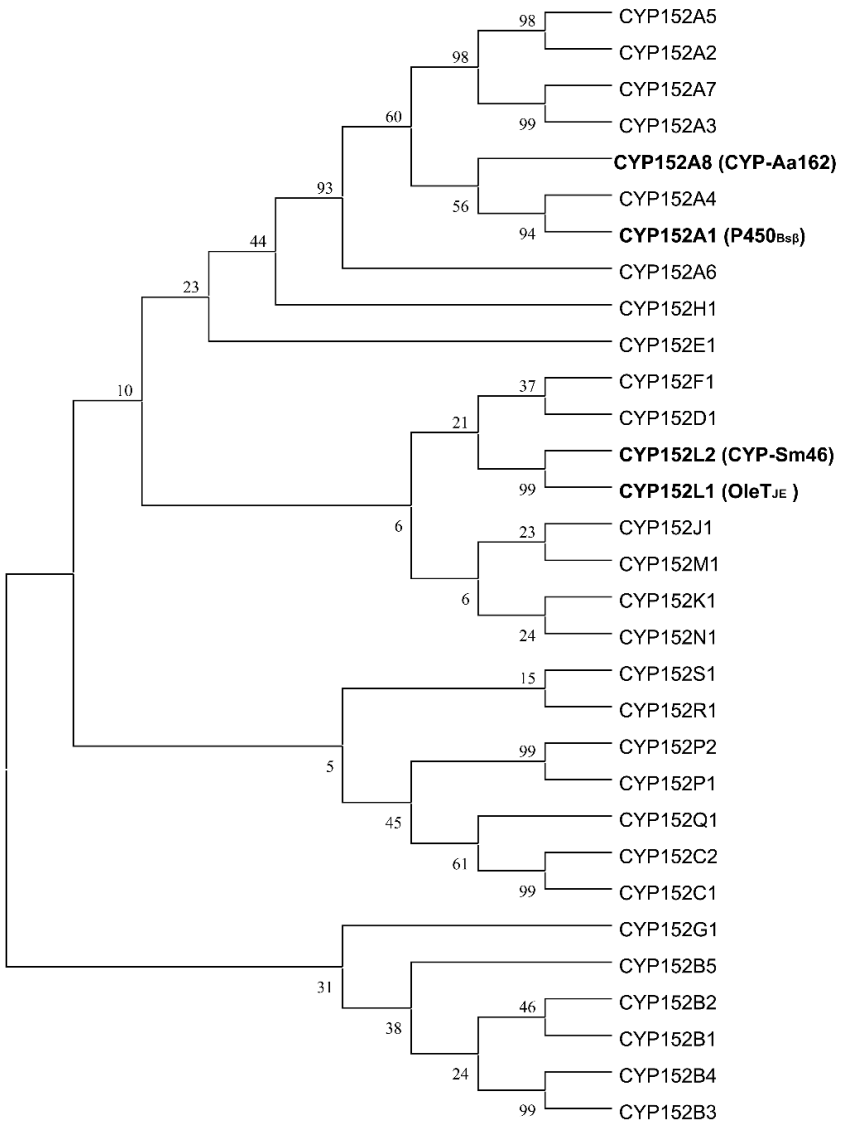

Figure S7. Phylogenetic tree for CYP-Aa162, CYP-Sm46Δ29 and other CYP152 family members. The sequences were aligned using Clustal W. The Neighbor-joining Tree was generated using MEGA 7.0 package. Bootstrap values shown next to the branches were computed from 1000 bootstrap tests. CYP-Sm46 is most closely related to the P450 fatty acid decarboxylase $OleT_{JE}$ (CYP152L1), while CYP-Aa162 (CYP152A8) is much closer to the P450 fatty acid hydroxylase $P450_{BS\beta}$ (CYP152A1).

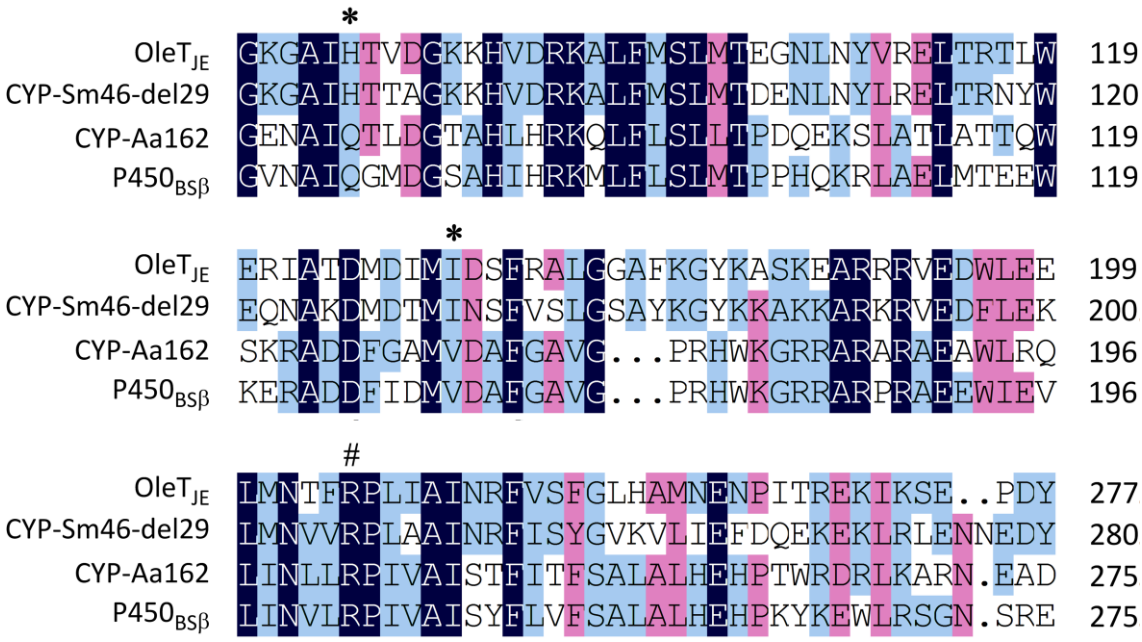

Figure S8. Protein sequence alignment of OleT$_{JE}$, CYP-Sm46Δ29, CYP-Aa162 and P450$_{BS\beta}$. *: the only two residues that are distinct in the active sites of these four P450 peroxygenases, which are proposed to be important for product distribution; #: the key catalytic residue.

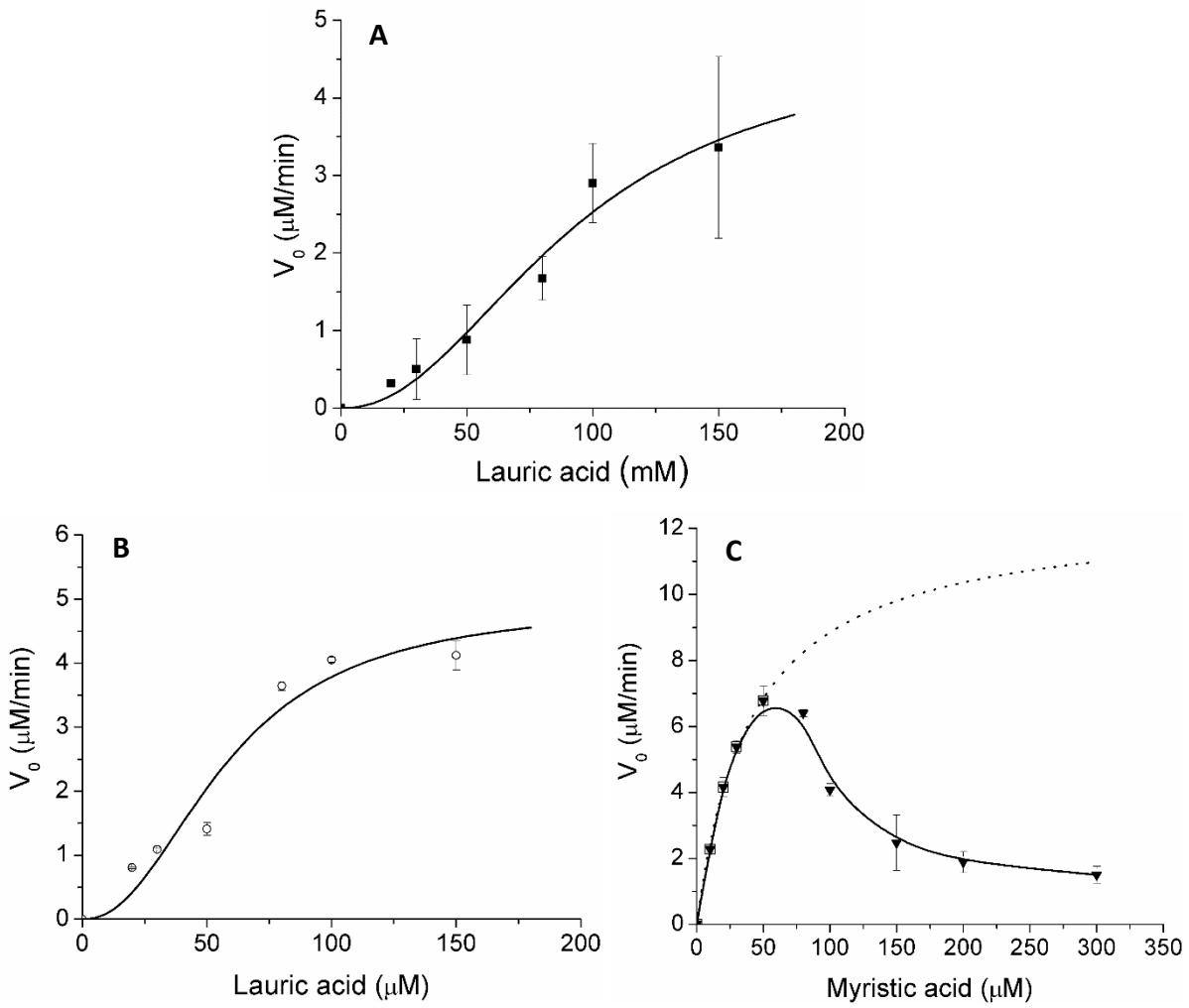

Figure S9. Kinetic curves of CYP-Aa162 and CYP-Sm46Δ29 against their optimal fatty acid substrates. (A) C_{12} lauric acid substrate consumption rates by CYP-Aa162 were fitted to Hill equation; (B) 1-undecene formation rates by CYP-Sm46Δ29 were fitted to Hill equation; (C) Solid line: the plot of 1-tridecene formation rates by CYP-Sm46Δ29 as a function of increasing C_{14} myristic acid concentrations, demonstrating substantial substrate inhibition. Dotted line: a hyperbolic curve fitted with Michaelis-Menten equation after truncating the inhibited rates at high C_{14} substrate concentrations. The steady state kinetic parameters were calculated using OriginPro 8.0 and are summarized in Table 2.